DOI: 10.1111/jiec.70087

RESEARCH ARTICLE

JOURNAL OF INDUSTRIAL ECOLOGY WILEY

Modeling material flow dynamics in coupled natural-industrial ecosystems for resilience to climate change

A case study on a soybean-based industrial ecosystem

William Farlessyost[1] | **Shweta Singh**[1,2,3]

[1]Agricultural and Biological Engineering, Purdue University, West Lafayette, Indiana, USA

[2]Environmental and Ecological Engineering, Purdue University, West Lafayette, Indiana, USA

[3]Davidson School of Chemical Engineering (By Courtesy), Purdue University, West Lafayette, Indiana, USA

Correspondence
Shweta Singh, Agricultural and Biological Engineering, Purdue University, West Lafayette, Indiana, USA.
Email: singh294@purdue.edu

Editor Managing Review: Stefan Pauliuk

Funding information
Division of Chemical, Bioengineering, Environmental, and Transport Systems, Grant/Award Number: FMRG ECO 2229250; National Science Foundation Graduate Research Fellowship Program, Grant/Award Number: DGE-1842166; US National Science Foundation through NSF GRFP, Grant/Award Numbers: DGE-1842166, NSF FMRG Eco 2229250

Abstract

Industrial ecosystems are coupled with natural systems, which causes the material flow dynamics in the network to be affected by the mechanistic dynamics of each node. However, current material flow dynamics studies do not capture these mechanistic and nonlinear dynamics to evaluate material flows in networks, thus missing its role in designing resilient industrial ecosystems. In this work, we present a methodology to overcome this limitation and model material flow dynamics in a coupled natural-industrial network by accounting for underlying nonlinear dynamics at each node. We propose a three-step methodology: first, creating accurate surrogate models using liquid time-constant (LTC) neural networks to capture node-specific behavior; second, coupling these individual node models to simulate material flow dynamics in the network; and third, evaluating resilience by measuring the system's ability to maintain production levels under climate stress. Applied to a soybean-based biodiesel production network in Champaign County, Illinois (2006–2096), our analysis reveals significant vulnerability differences between climate scenarios, with the RCP 8.5 scenario triggering production failures approximately 10 years earlier than RCP 4.5 (2016 vs. 2026), exhibiting higher failure frequency and requiring longer recovery periods. Smaller farms (450 ha) demonstrated substantially higher import dependency, while medium farms (500 ha) reached a critical bifurcation point around 2050 under RCP 8.5, indicating a systemic tipping point. These findings provide insights for policymakers and industrial managers to implement targeted interventions, supply chain diversification, and adaptive management strategies, thereby enhancing system resilience while offering industrial ecology practitioners a methodology for modeling material flow dynamics in a coupled natural-industrial network.

KEYWORDS
climate change, coupled industrial natural systems, machine learning, material flow dynamics, resilience, surrogate modeling

1 | INTRODUCTION

Climate change poses significant challenges to global food security and sustainable energy production, necessitating a deeper understanding of coupled natural–industrial systems' resilience (Dijkema et al., 2015; Meerow et al., 2015). The increasing frequency and severity of extreme weather events, shifts in precipitation patterns, and rising temperatures are altering the fundamental dynamics of agricultural ecosystems (Anjum et al., 2019; Bekele et al., 2021; Huang et al., 2020; José et al., 2016; Kim et al., 2013; Nasonova et al., 2018; Nilawar & Waikar, 2019; Wang et al., 2020; Zhang et al., 2016). These changes have far-reaching implications for crop yields, water availability, and the overall stability of food production systems. As climate variability intensifies, it becomes crucial to develop robust methodologies for assessing and predicting the impacts on interconnected natural and industrial ecosystems on material flows and demands, particularly in the context of agricultural value chains and their associated energy production systems.

Industrial ecosystems, particularly those centered around agricultural production and processing, are inextricably linked with natural systems through complex feedback and dependencies for raw materials (Costa et al., 2019; Meerow et al., 2015). These coupled natural–industrial systems exhibit highly intricate and nonlinear dynamics driven by diverse interacting factors ranging from resource constraints to market forces (Dijkema et al., 2015; Meerow et al., 2015). For instance, in the case of biofuel production, the industrial ecosystem encompasses not only the manufacturing processes but also the agricultural systems that supply the raw materials. This coupling manifests through various pathways, including land use changes, water consumption, nutrient cycling, and energy flows. The interdependencies between crop growth, harvesting, processing, and end-product distribution create a network of interactions that span multiple spatial and temporal scales, making these systems particularly vulnerable to climate-induced perturbations.

The cascading effects of climate change–induced disruptions in natural systems can significantly impact the stability and efficiency of industrial ecosystems. As climate variability alters crop growth patterns, yield potentials, and water availability, these changes propagate through the entire value chain, affecting industrial processes, resource allocation, and ultimately, product output (Beck et al., 2018; Rogelj et al., 2012). For example, shifts in temperature and precipitation regimes can lead to changes in crop phenology and productivity, which in turn influence the timing and availability of volume of raw material inputs to processing facilities (Costa et al., 2019; Padhiary & Kumar, 2024; Padhiary et al., 2025). This can result in supply chain disruptions, necessitating adaptive measures in industrial operations. Moreover, extreme weather events can cause acute shocks to the system, potentially leading to crop failures or infrastructure damage that ripple through the interconnected network of agricultural and industrial processes. Understanding these cascade effects on material flows is crucial for developing resilient and sustainable industrial ecosystems in the face of ongoing climate change.

Material flow analysis (MFA) has been widely used to quantify the environmental impacts and resource flows within these systems (Cioni, 2002; Graedel, 2019; Pauliuk et al., 2015; Sendra et al., 2007). These approaches provide valuable insights into the overall sustainability and efficiency of industrial processes, including their interactions with natural ecosystems. For instance, MFA allows for tracking material and energy flows across the industrial ecosystem, revealing potential inefficiencies and connections with environmental systems. While the static MFA offers a comprehensive snapshot of system performance for resource utilization, it often struggles to fully capture the dynamic nature of climate-induced disruptions and the resulting cascade effects on coupled natural-industrial systems (Harirchi et al., 2020; Rivera, 1996; Rivera et al., 2003). Dynamic material flow analysis (DMFA) offers insights into temporal changes in material stocks and flows, but can be limited in capturing complex feedback mechanisms and non-linear behaviors in coupled systems (Cao et al., 2018; Espinoza et al., 2014; Müller et al., 2004; Xu et al., 2024) unless mechanistic details of processes are included in the projection. As most DMFA models are either input-driven or output-driven with a simple relationship between the stock and flows, these do not necessarily capture the complex interactions within coupled natural-industrial systems that can account for intricate multiscale dynamics (Streeck et al., 2023). These systems exhibit behaviors that span various temporal and spatial scales, from rapid biochemical reactions in crop growth to biophysical reactions driven by industrial dynamics. Capturing these multiscale dynamics is crucial for understanding system resilience and predicting responses to climate change. For example, short-term weather fluctuations can impact daily crop water requirements, while long-term climate shifts may alter entire growing seasons and crop suitability in a region. Similarly, industrial processes may have immediate responses to input variations, as well as long-term adaptations to persistent changes in raw material quality or quantity. Integrating these diverse scales of interaction is essential for a comprehensive understanding of system behavior under different climate change scenarios (Davis et al., 2009; Meinrenken et al., 2014).

To address this critical gap and overcome the lack of inclusion of mechanisms impacting multiscale dynamics of material flows, our study presents a broad framework for modeling these coupled material flow dynamics using a system identification–based approach (Figure 1). This novel methodology aims to capture complex, nonlinear dynamics across entire industrial ecosystems, offering a more comprehensive understanding of material flow dynamics driven by mechanisms at each node. The proposed approach utilizes a system identification approach of key system components to build surrogate models, which are then used to model the network interactions, facilitating a more accurate representation of the coupled natural-industrial ecosystems dynamics.

To implement this system identification-based approach, we leverage surrogate modeling techniques, specifically using data-driven liquid time constant (LTC) neural networks (Hasani et al., 2021). Surrogate models provide computationally efficient approximations of complex underlying

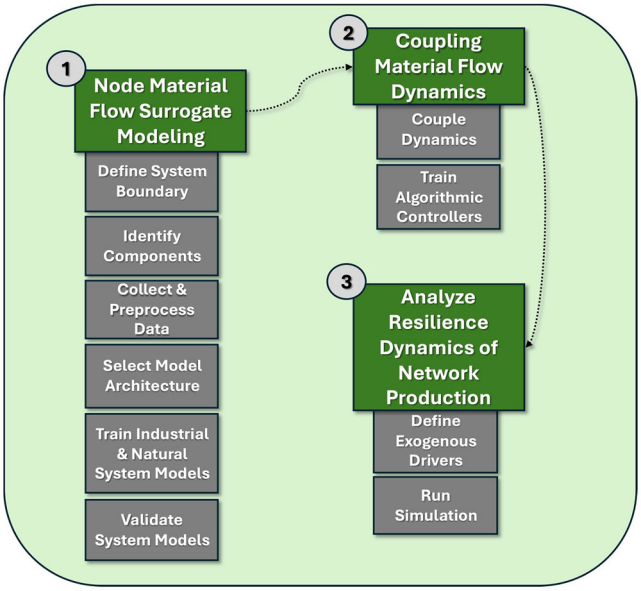

FIGURE 1 Methodology for modeling, coupling, and simulating material flow dynamics under the effects of exogenous drivers (economics, climate, etc.).

processes, allowing for rapid scenario analysis and system-wide simulations that would be impractical with full mechanistic models. LTC neural networks offer unique advantages in capturing temporal dynamics and nonlinear behaviors inherent in coupled natural-industrial ecosystems (Hasani et al., 2020; Lechner et al., 2020). These networks employ "liquid" neurons with dynamic time constants, enabling the capture of complex temporal contexts and nonlinear dynamics without the computational burden of full mechanistic simulations. By training these LTC models on synthetic data generated from high-fidelity simulations, we combine the detail of mechanistic models with the efficiency of more abstract representations (Bidollahkhani et al., 2023). This novel combination provides crucial supervision and regularization, allowing the model to converge on meaningful causal relationships while avoiding the parameter uncertainties and computational limitations often encountered in fully mechanistic approaches (Hasani et al., 2022; Lechner et al., 2020). These models can then be used to study material flow dynamics in the network under various climate change scenarios for evaluating the resilience of the network to climate change. In this context, we define resilience as the system's ability to maintain industrial production above a critical threshold given an exogenous climate shock. We assess resilience dynamics using failure frequency, system recovery time, and ID of tipping points. The key questions addressed in this paper are:

1. How well do LTC-based surrogate models approximate the material flow dynamics of agricultural-industrial nodes compared to mechanistic simulations of these systems?
2. How to account for dynamics and external influence on material stock accumulation in the network and subsequent node production?
3. How can we utilize simulation of material flow dynamics in the coupled natural–industrial ecosystem for analysis of resilience?

To demonstrate the proposed methodology and address our questions, we present a case study focusing on a soybean-based biodiesel industrial ecosystem in Champaign County, Illinois. This coupled natural–industrial ecosystem encompasses the value chain, from soybean agriculture to biodiesel production. The IE in this case consists of manufacturing nodes representing soybean oil extraction and biodiesel production processes. We apply the LTC modeling approach to create surrogate models that efficiently simulate the growth patterns of soybean crops, soybean oil production, and conversion to soybean biodiesel. These surrogate models are driven by statistically downscaled climate projections from 2006 to 2096 under two scenarios: Representative Concentration Pathway (RCP) 4.5 and 8.5 (Riahi et al., 2011). This setup enables us to analyze potential future climate impacts on crop yields and subsequent cascading effects on stocks & flows throughout the integrated system with a level of computational efficiency that allows for extensive exploration of scenarios and sensitivities.

The remainder of this paper is structured in the following way. Section 2 describes our methodology in detail, outlining the steps for system boundary definition, component system identification, data collection and preprocessing, model architecture and training, and the coupling of dynamics across the natural-industrial ecosystem. We also discuss the training and implementation of LTC inverse models as algorithmic plant controllers and the generation of exogenous climate and economic demand signals. Section 3 presents the case study setup, detailing the specific components of the soybean biodiesel industrial ecosystem in Champaign County, Illinois, and provides a comprehensive analysis of our results, discussing the simulation outputs that assess production rates, waste generation, stock levels, and required imports under RCP 4.5 and 8.5 scenarios

for varying farm sizes. We evaluate the system's resilience and sustainability under different climate projections and discuss the implications of our findings. Finally, Section 4 summarizes the key insights, addresses limitations, and suggests directions for future research for modeling material flow dynamics in coupled natural-industrial ecosystems.

2 | METHODS

To address the three research questions, our proposed approach has three specific parts: (1) surrogate modeling for estimating material flow dynamics of nodes; (2) material flow dynamics in coupled natural-industrial network system, and (3) evaluating resilience dynamics to maintain production in coupled natural—industrial network system, as shown in Figure 1.

2.1 | Surrogate models for estimating material flow dynamics of nodes

We first develop an approach to generate surrogate models that can estimate the material flow dynamics of nodes, capturing the underlying mechanisms of the node.

2.1.1 | System boundary

We start by defining a system boundary to demarcate the spatial regions of interest, ensuring that all industrial operations and natural ecosystem dynamic processes and interactions of interest are encapsulated while extraneous influences are excluded. Throughout, the spatial boundary is the Champaign County line; any flow that crosses this line is logged as an import (positive) or export (negative). Industrial operations usually entail various production processes, and thus, the system boundary should delineate the specific life cycle stages. Natural ecosystems reflect the dynamics of relevant crops with plant growth or other environmental processes, considering environmental variables that influence growth patterns and serve as the principal dynamic drivers. Dynamic processes and interactions from either natural or industrial systems for which data do not exist to build state-accurate models should be excluded from the system boundary; however, their impact can be considered as an exogenous perturbation to the system. Care is taken to ensure the system boundary remains realistic over whatever time intervals are considered as the period of analysis (Nabavi et al., 2018).

2.1.2 | Component identification

Identifying and understanding the individual components within the system boundary is paramount for a thorough analysis. This involves breaking down the system into discrete nodes or units, each representing a specific process or entity with clearly defined inputs and outputs, either from or to another node, or from or to an exogenous source/sink. For instance, in an industrial setting, nodes represent distinct production stages or units with feedstock and material flow rates, while in a natural ecosystem, nodes signify the growth of species or natural material availability over time, given changes in environmental conditions exogenous to the system or anthropomorphic waste flows.

2.1.3 | Data collection and preprocessing

Further, understanding the characteristics of each node allows us to choose the appropriate data on which to train individual node models. The emphasis throughout this process is to ensure that the data are both representative of the real-world dynamics of the node and are structured in a way that is conducive to effective modeling. Proper preprocessing not only enhances the accuracy of the models but also contributes to their generalizability across different scenarios or conditions. Data can be sourced from a combination of experimental datasets, historical records, and synthetic data generated from mechanistic models. Depending on the specific node in question, this will involve time-series data capturing dynamic changes, cross-sectional data detailing model parameterization in specific instances, or even qualitative data that are subsequently quantified for modeling purposes to scale the data/model. In our approach, we mainly rely on mechanistic simulation models to generate synthetic data to capture material flow dynamics based on underlying governing principles at each node.

Given the diverse sources of data and the potential variations in scales, units, or magnitudes, standardizing or normalizing the data prior to use in training becomes imperative. This ensures that no feature or variable disproportionately influences the model. Techniques like *z*-score

normalization or min–max scaling are employed based on the data distribution. Additionally, in datasets with high noise, smoothing techniques, such as rolling averages, might be applied where appropriate to focus on underlying trends or patterns.

2.1.4 | Model architecture and training

Building an accurate model for node dynamics necessitates a careful selection of model architecture and a structured training process that may vary from node to node. The following outlines the general approach to model architecture and training.

Suitable model architecture should be chosen depending on the nature and characteristics of the node system. The primary criterion for model selection is its ability to capture the underlying patterns and dynamics of the node in question and predict the dynamics of the modeled outputs given a set of input dynamics; second is the interpretability/auditability of the model structure and parameterization.

Available datasets for each node are partitioned into training, validation, and testing subsets, following standard machine learning methods. The training set is used to adjust the model's parameters, the validation set aids in hyperparameter tuning and to prevent overfitting during training, and the testing set provides an unbiased performance evaluation. Training is iterative, where the model is exposed to the data multiple times (epochs), refining its weights and biases to minimize the discrepancy between its predictions and actual values. We use mean average error (MAE) as the loss function defined as for a dataset with n observations, where $y_{)}$ represents the actual value and $\hat{y}_{)}$ represents the predicted value, as:

$$\mathrm{MAE} = (1/n) \times \Sigma \left| y_{(i)} - \hat{y}_{(i)} \right| \text{ for } i = 1 \text{to } n. \tag{1}$$

2.1.5 | Model evaluation

The evaluation process not only gauges the model's performance on unseen data but also informs potential refinements or improvements so that the developed model is robust, accurate, and generalizable. Each node model is integrated or computed over time, and the output is compared against the ground truth data trajectory (test data).

We employ a summary quantitative metric of root mean square error (RMSE) in Equation (1). RMSE is defined for a dataset with n observations, where $y_{)}$ represents the actual value and $\hat{y}_{)}$ represents the predicted value, as:

$$\mathrm{RMSE} = \sqrt{\left((1/n) \times \sum \left(y_{(i)} - \hat{y}_{(i)} \right)^2 \right)} \text{ for } i = 1 \text{ to } n. \tag{2}$$

This metric provides a measure of the model's ability to make accurate predictions that can be easily compared. However, beyond quantitative metrics, visual inspections play a crucial role in understanding the model's performance. By plotting actual versus predicted values, inconsistencies, outliers, or patterns of discrepancies is visually identified. These plots offer an intuitive understanding of where the model excels and where it may falter and should be improved. This is especially useful in scenarios where quantitative metrics might not capture nuanced discrepancies or where the nature of errors is as important as their magnitude.

2.2 | Material flow dynamics in a coupled natural–industrial network system

Next, we address the question of accounting for the dynamics of coupled natural–industrial networks on material flows and accumulation. To answer this, we use the coupling of nodes to simulate coupled dynamics, similar to the system dynamics approach. However, we additionally design controllers to adjust the flow between nodes as per the driving factor change.

2.2.1 | Node coupling

It is crucial that all interactions between the industrial and natural components identified as nodes within the system boundary are appropriately characterized through node-to-node coupling of dynamics. Each node's output is identified and mapped to serve as the direct input for a subsequent node or nodes, or an exogenous sink outside the system boundary. Likewise, each node input is either mapped as the output of another node or an exogenous source. Consequently, it is vital that all node models and exogenous data sources are on the same timescale. To this end, retiming or interpolation of either a model or data may be necessary to achieve this.

While not a significant factor in our specific case study, it is necessary to mention there are scenarios where the transmission of an output from node A to the input of node B might be heavily delayed or have significant consequences in the overall system dynamics. Such delayed responses can be accounted for, ensuring that the system's dynamics capture these temporal lags. Methods range from adding a simple time-delayed lag into a signal's time-series feed to building an additional dynamic model to approximate this lag from known data.

2.2.2 | Algorithmic controllers in node integration

Within the context of the simulated system, we suggest that inverse model "controllers" be employed as algorithmic constructs that ensure the right balance between demand and the necessary feedstock for industrial nodes. By adjusting inputs based on real-time simulated demand, the system can emulate the adaptive nature of real-world industrial processes seeking to produce enough to hit that changing demand.

Therefore, the controllers should continuously monitor the simulated economic production demand and, based on the current demand and set-point values, the algorithmic controllers fine-tune the feedstock quantities. This ensures that the simulated industries operate in line with their demand profiles, even in scenarios where there are fluctuations or changes in the demand. Outputs from industrial nodes, regulated by these algorithmic controllers, serve as inputs to subsequent nodes or systems in the simulation. By embedding these algorithmic controllers within the simulation, the methodology ensures that each node or industrial process is responsive and adaptive, reflecting the dynamic interplay between demand and supply in a realistic manner for the material flows in coupled network systems.

2.3 | Evaluating network production resilience with dynamics

2.3.1 | Simulation of exogenous disruptors and economic demand scenarios

Understanding how the coupled natural–industrial ecosystems respond to external scenarios, especially those that vary depending upon the placement and drawing of the system boundary spatially, is necessary for gauging their resilience and overall sustainability. To this end, we suggest supplying two types of exogenous time-series inputs to the system: *disruptive signals* and *economic demand signals*. "Disruptive signals" propagate the dynamics of a process or event that might have disruptive consequences on a system node (e.g., drought, flooding, infrastructure damage, etc.) through the system via the information as node input. "Economic demand signals" function as the production goal of the network over time. These signals are passed to the algorithmic controllers, which translate them into feedstock requirements for each of the industrial node models to meet demand. Depending on the node or component, these external forces might directly influence production rates, resource availability, or even operational feasibility. Depending on the focus of the study, the simulation may be run over varying time horizons. Short-term simulations might capture immediate system responses, while long-term simulations can provide insights into cumulative effects and potential tipping points.

2.3.2 | Evaluating system resilience

We assess the system's resilience, here defined as its ability to maintain production matching the economic demand signal given the exogenous disruptor signal, using the generalized approach given in Figure 2. The metrics used are potential weaknesses, tipping point, and failure recovery time. Here, *potential_weaknesses* are periods when stock levels approach depletion thresholds given in Equation (1) as:

$$W_{\mathrm{p}} = S_{\mathrm{min}}/Sc_{\mathrm{u}} \tag{1}$$

where S_{min} is the critical minimum stock level, and Sc is the current stock level.

A *tipping_point* (Equation 2) marks the point when stock levels supplying feedstock to the plant dip below the minimum threshold and never recover:

$$t_{\mathrm{tip}} = \min\{t : S(t) < S_{\mathrm{min}} \forall\, t \geq t_{\mathrm{tip}} \tag{2}$$

The duration required for production to recover to its baseline level after a failure event is given in Equation (3) and referred to as the *failure_recovery_time*:

$$T_{\mathrm{r}} = t_{recover} - t_{fail} \tag{3}$$

```
// 1. Define minimum and maximum acceptable thresholds for each stock variable or reservoir
FOR EACH stock_variable IN system
   DEFINE min_threshold, max_threshold
   // These thresholds represent levels below which production might be compromised
   // or above which there might be wastage or inefficiencies
END FOR
// 2. Track stock level fluctuations in response to the disruptor signal
FOR EACH stock_variable IN system
   MONITOR stock_level
   IF stock_level DEVIATES significantly FROM min_threshold OR max_threshold THEN
      IDENTIFY system vulnerabilities OR inefficiencies
   END IF
END FOR
// 3. Evaluate stock variables as buffers against sudden changes in demand or supply
FOR EACH stock_variable IN system
   ASSESS buffer_capacity
   IF stock_variable ABSORBS disruptions WITHOUT affecting production THEN
      CLASSIFY stock_variable AS robust
   ELSE
      NOTE potential for wastage OR inefficiencies
   END IF
END FOR
// 4. Track production rates of nodes in the network throughout the simulation
FOR EACH node IN network
   TRACK production_rate DURING simulation
   IF production_rate IS consistent EVEN in adverse scenarios THEN
      INDICATE strong system resilience
   ELSE
      FLAG potential weaknesses
   END IF
END FOR
// 5. Measure quantities and frequencies of imports required to maintain stability and production levels
TRACK import_quantities, import_frequencies
IF imports ARE frequent OR large THEN
   INDICATE system vulnerabilities OR deficiencies
END IF
// 6. Identify tipping points where the system might bifurcate from a stable state to failure
FOR EACH stock_variable IN system
   FOR EACH node IN network
      IF stock_levels OR production_rates REACH critical levels THEN
         IDENTIFY tipping_point
      END IF
   END FOR
END FOR
// 7. Evaluate waste generation trends within the system
TRACK waste_generation
FOR EACH stock_variable IN system
   IF unused_stock IS generated AND exceeds acceptable levels THEN
      IDENTIFY inefficiencies OR overestimations in stock procurement
   END IF
END FOR
```

FIGURE 2 System resilience assessment methods.

where t_{fail} is the timestep when production falls below a critical threshold (failure event), and $t_{recover}$ is the timestep when production returns to the baseline level.

3 | Results

We apply our proposed methodology to evaluate the resilience of a coupled natural–industrial ecosystem shown in Figure 3. In this network, industrial systems of soybean oil and soybean biodiesel are coupled with the natural system of soybean farming, thus forming a coupled natural–industrial ecosystem. Further, we test the resilience of this network to climate change disruptions under RCP 4.5 and 8.6 for meeting the simulated economic

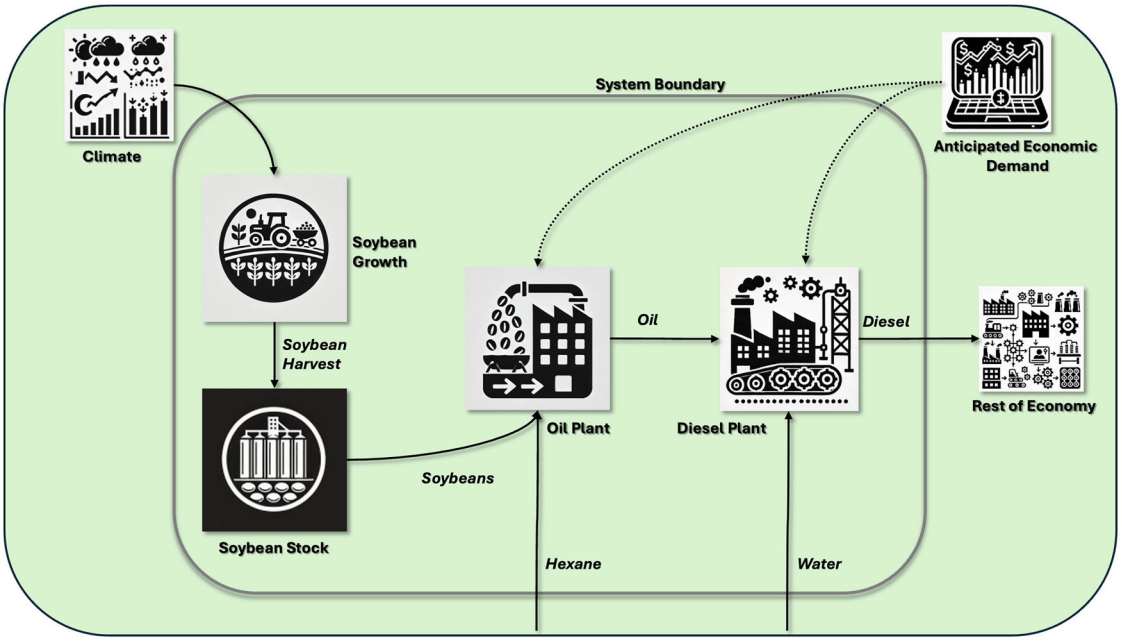

FIGURE 3 All flows are shown in kg h^{-1}. Hypothetical soybean network in Champaign, Illinois, subject to anticipated exogenous economic demand (information) and changes in climate (physical) over time. The system boundary is drawn to include nodes of soybean growth and oil and diesel production shown in the inner box(gray ring).

demand scenarios (Figure 4). We show the system boundary, results on training a surrogate model for node dynamics and coupled dynamics under climate change impact here. The details of data generation, preprocessing, and economic and climate forecasts are provided in the first and second sections of Supporting Information S1.

3.1 | Surrogate models for soybean diesel production network node dynamics

3.1.1 | System boundary and component identification

Spatially, our system boundary is drawn to encapsulate the area directly surrounding Champaign, Illinois, in the United States. The system boundary includes soybean agricultural production as well as derivative products of oil and diesel. The soybean production network works to meet the external economic demand for diesel, while also being impacted by the exogenous disruption of changing climate conditions, affecting the growth of soybeans.

At the heart of the network lie three dynamic nodes, as shown in Figure 3. These nodes represent distinct life cycle stages in the soybean biodiesel production.

Soybean growth: This node models the seasonal growth of soybeans, with dynamics heavily influenced by climate variables of temperature, precipitation, and solar radiation. The culmination of this stage is the harvest, with the yield being transferred to an inventory stock. Our analysis considers soybean farms of 450, 500, and 550 hectares in size to determine their relative effects on network production resilience.

Soybean oil plant: The node dynamics here consist of solvent extraction using hexane to convert soybeans from the inventory into crude soybean oil. An important by-product of this stage is soybean meal, which is tracked but not considered further in our analysis.

Soybean diesel plant: The culmination of the value chain, this node takes the crude soybean oil and, in conjunction with water, processes it into diesel fuel via trans-esterification. This diesel is passed to some exogenous demand sink outside of the system boundary, consistent with the anticipated economic demand signal passed to the network.

A *soybean stock* is employed as the difference between yearly soybean harvest added and soybean feedstock utilized for oil over time, making it a dynamic entity coupling the soybean agricultural growth with the industrial oil and diesel production. It also acts as a buffer, whose level determines whether the soybean oil production node has a consistent supply, ultimately leading to a steady production of soybean diesel. However, stock that accumulates and is not used within a 3-year period is removed and sent to *waste*.

Several assumptions are made about network operation to simplify the analysis. First, soybean growth is assumed to be homogenous across the farm, and the harvest time does not change year to year. All harvested soybeans are accumulated in the soybean stock, and the soybean plant is the only recipient of this stock. Further, all soybean oil is used in the production of soybean diesel, and all soybean diesel produced goes to satisfy

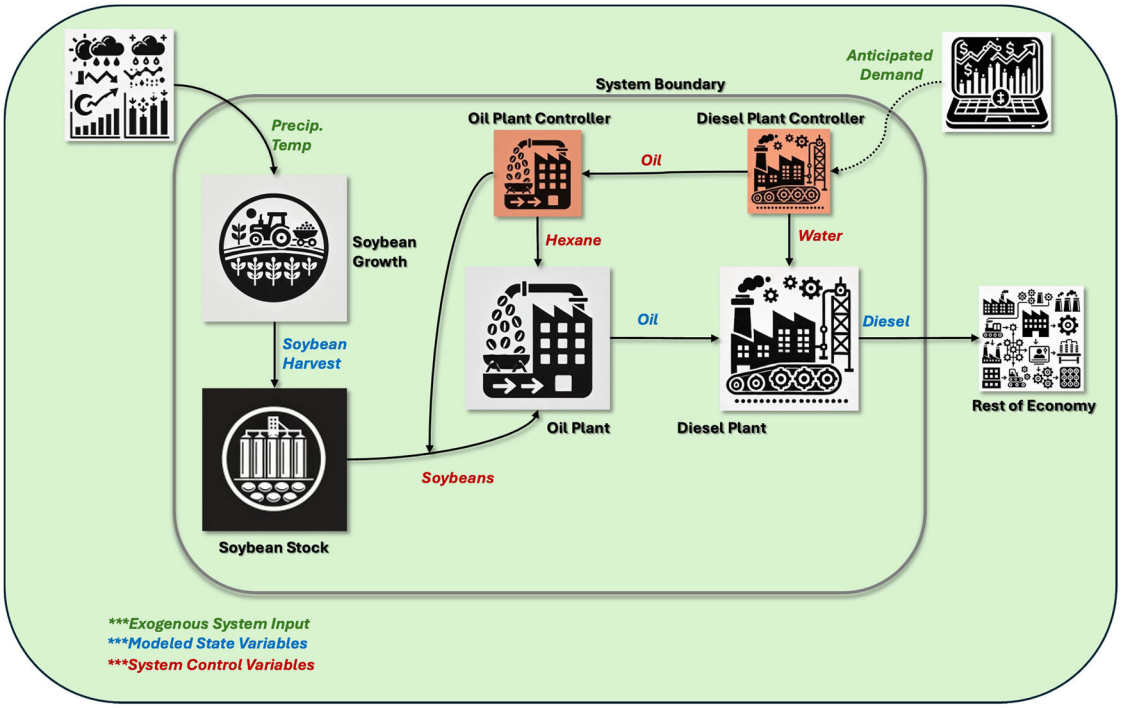

FIGURE 4 Soybean network with algorithmic controllers in place to control oil and diesel production. Green streams are exogenous inputs to the industrial network (climate change and increasing economic demand). Blue streams are material flows out of nodes with dynamics modeled with LTC-NNs. Red streams are material flows predicted as feedstock requirements for oil and diesel production nodes by the inverse model (LTC) controllers based on anticipated economic demand for soybean diesel. All flows are shown in kg h^{-1}.

exogenous economic demand. Other necessary feedstocks that vary dynamically over time (i.e., water and hexane) are considered as exogenous sources, whose utilization is not tracked as part of this analysis.

3.1.2 | Data collection and node model architecture

Our modeling approach for the industrial and natural dynamic nodes utilizes LTC neural networks. Three different types of neurons make up each model. Input neurons in an LTC network are designed to interface with the environment, receiving external time-varying signals. Unlike traditional artificial neurons, LTC input neurons can handle continuous-time inputs, which allows them to process information that changes over time, such as the varying rates of soybean and hexane input in a soybean oil plant. Hidden neurons in LTC networks each use a liquid time-constant based on the current input and state of the network, allowing the neuron to adapt its response over time. Output neurons, or motor neurons, in an LTC network generate the final output signals that control actions or make predictions based on the processed inputs and the learned temporal dynamics (Davis et al., 2009). In the context of the soybean oil and biodiesel plant models, motor neuron output signals correspond to the production rates, whereas in the agricultural model, the motor neuron is the soybean accumulated mass.

Industrial system node models

For the soybean oil plant, the input nodes consist of soybean and hexane (Figure 3). In the case of the biodiesel plant, the inputs are water and soybean oil. The hidden nodes, which serve as the intermediary layer in both models, are determined through an iterative process. The number of hidden neurons is increased until the integrated model no longer approximates a horizontal line. Finally, the motor neurons are selected based on their value-added significance and the necessity for a proper model fit. For the soybean oil plant, the outputs are soybean oil and soymeal, while for the biodiesel plant, the outputs are diesel and an oil recycling stream internal to the plant.

Natural system node model

For the modeling of soybean growth, the LTC neural network is configured with an emphasis on key environmental variables. The inputs to this model are time, precipitation, and temperature. These sensory neurons were selected through an iterative process seeking to reduce the number of model inputs without wrecking model performance, while holding the number of hidden neurons constant (31 hidden neurons with 1 motor

neuron). With inputs determined, the hidden layer, composed of 20 neurons, was determined through an iterative approach akin to that utilized for industrial plant modeling. At the output layer, a single motor neuron corresponds to the overall soybean mass over time.

3.1.3 | Model training

The four LTC models are trained on the synthetic data discussed previously with an 80–20 training-to-testing split. The soybean oil and diesel production plant models were thus each trained across 8000 h of data, while the soybean growth, with different models for each RCP 4.5 and 8.5, was trained across 72 growing seasons (also at hourly resolution).

The training loss for the soybean oil LTC model, shown in Figure 4 of Supporting Information S1, exhibited a rapid decline during the initial stages. Convergence of the loss (Equation 1) was indicated as the loss plateaued around 125 epochs. To mitigate the risk of overfitting due to inherent noise within the training data, training was curtailed at this juncture.

Akin to the soybean oil production model, the biodiesel production LTC model's training loss saw a swift reduction, stabilizing around the 125-epoch mark. Training was subsequently terminated to avert potential overfitting.

Distinctively, the soybean growth LTC model's training loss experienced a sharp decrease post the inaugural pass through the multi-year seasonal dataset. The loss consistently remained below a 0.01 mean squared error in the ensuing cycles, displaying a discernible repetition around the 400th step. Given the overarching goal to thwart potential overfitting, training was concluded at 200 steps.

3.1.4 | Model evaluation

The LTC node models were rigorously evaluated against 20% of the soybean growth synthetic data (18 growing seasons) to gauge their proficiency in capturing the complex dynamics of the soybean production system. The models are integrated over time and compared against this test data in Figure 5 of Supporting Information S1.

The soybean diesel model shows a good fit with an RMSE of 0.11 on the test data. Noteworthy was its capability to accurately pinpoint key inflection points and shifts within the diesel production time series. However, achieving the absolute correct value of local extrema throughout the time series remained elusive. With a test RMSE of 0.194, the soybean oil LTC model's performance was congruent with the diesel model, demonstrating adeptness at capturing trend reversals.

The soybean growth model rendered an RMSE of 0.105 on the test set, shown in Figure 5 of Supporting Information S1. The model's predictions of soybean accumulated mass did exhibit sporadic oscillations, particularly before the onset of full germination and during intervals characterized by swift growth. Nonetheless, its predictions closely aligned with the long-term mass trajectory, effectively identifying pivotal moments of crop maturity and peak harvest mass. Full training residual plots are shown in Figure 4 of Supporting Information S1.

3.2 | Material flow dynamics in soybean diesel production network

3.2.1 | Node coupling and algorithmic controller for node integration

In the framework presented, algorithmic controllers serve as integrators that balance material flows in the network in response to fluctuating demand. This allows for capturing the impact of fluctuation on the material flows within the network by capturing cascading mechanisms. In the network, we implement two such controllers as LTC inverse models to ensure that production meets demand. The oil plant controller regulates soybean and hexane feedstock inputs based on predicted oil demand, while the biodiesel plant controller adjusts soybean oil and water inputs to maintain stable biodiesel production levels.

The algorithmic controller LTC models are trained on top of the frozen weights of the LTC industrial plant models in the following manner (see Figure 5). First, the demand-required plant output time series is provided to the LTC controller as input-training data ("desired" input in Figure 5), and the prediction is then passed through the industrial models. Next, the MAE difference between the production output and the desired production (training data output) is taken as the loss function here, and the LTC controller model parameter weights are updated via back-propagation, while the LTC plant model weights are frozen and remain unchanged. The number of hidden neurons for each LTC controller is chosen iteratively in the same fashion as the LTC node models. This results in 8 hidden neurons in the oil plant controller and 12 in the diesel plant controller, likely the result of the greater complexity in the diesel plant processes. The motor variables chosen for each controller LTC model correspond to the plant feedstocks (soybean and hexane for the oil plant controller and oil and water for the diesel plant controller).

Both controllers have an additional input (Figure 5), soymeal desired and oil recycled desired for the oil and diesel plants, respectively, in addition to the main production signals that they are controlling for that is not included in the MSE loss calculation. The algorithmic controllers are trained

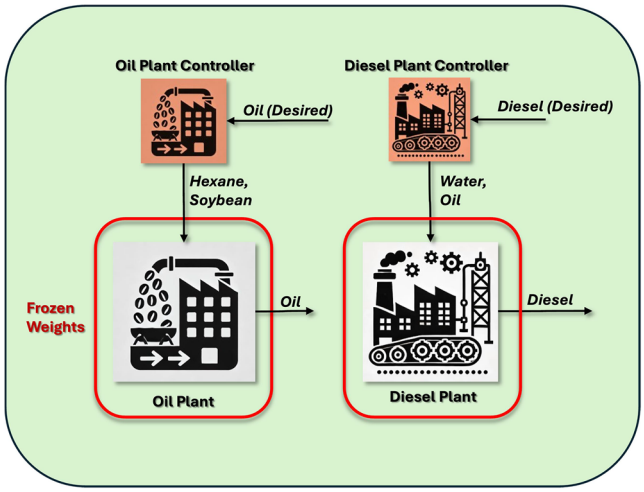

FIGURE 5 Soybean oil and diesel plant controllers (LTC models) trained on top of existing soybean oil and diesel plant LTC models. Note: LTC model controller weights are updated via back-propagation, while industrial plant LTC model weights are frozen (unchanged).

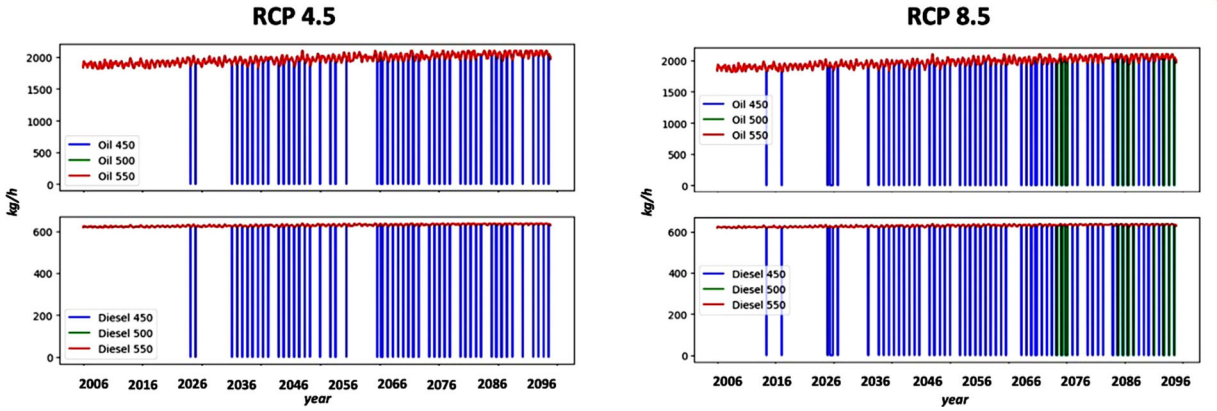

FIGURE 6 Network production during RCP 4.5 and 8.5 climate scenarios with 450, 500, and 550 ha soybean farms. Failure occurs when production drops to 0 kg h^{-1}. Failure recovery time is determined by how long production stays at 0 kg h^{-1}. The underlying data for this figure are available in Supporting Information S2.

over the same ASPEN Plus Dynamics synthetic data as the LTC plant models, following a similar 80–20 training-to-testing split using Python's timeseries split library. The LTC architecture for each algorithmic controller is shown in Figure 6 of Supporting Information S1.

Both the LTC models trained as oil and diesel algorithmic controllers were evaluated over the 2000 h corresponding to their industrial process.

The soybean oil algorithmic controller model achieved an RMSE of 0.13 on the test reference trajectory (Figure 7 of Supporting Information S1). Although it occasionally registered undershoots on outlier setpoints, it demonstrates swift reversion to optimal control values. Likewise, with an RMSE of 0.19 on the test set, the diesel algorithmic controller model echoed the robust performance observed in its counterpart, adeptly maintaining desired trajectories (Figure 7 of Supporting Information S1).

3.3 | Evaluation of soybean diesel network production resilience

Using the previously defined exogenous inputs to the system and coupled models, we evaluate the resilience of the integrated soybean production system and the dynamics across the entire life cycle stages, spanning from soybean growth to biodiesel production, under varying climate projections.

First, we focus on the network's material flow dynamics rate over the integrated time horizon of 2006–1996. As shown in Figure 6, several differences appear between the RCP 4.5 and RCP 8.5 scenarios as well as between the 450-, 500-, and 550-ha farms. At the same farm size, we see an increased failure frequency, indicated by dips to zero, an increase in required recovery time between RCP 4.5 and 8.5, as well as an earlier initial failure occurring around 2016 versus 2026. Further, only the 450-ha farm-supplied network exhibits failures during the RCP 4.5 scenario, whereas

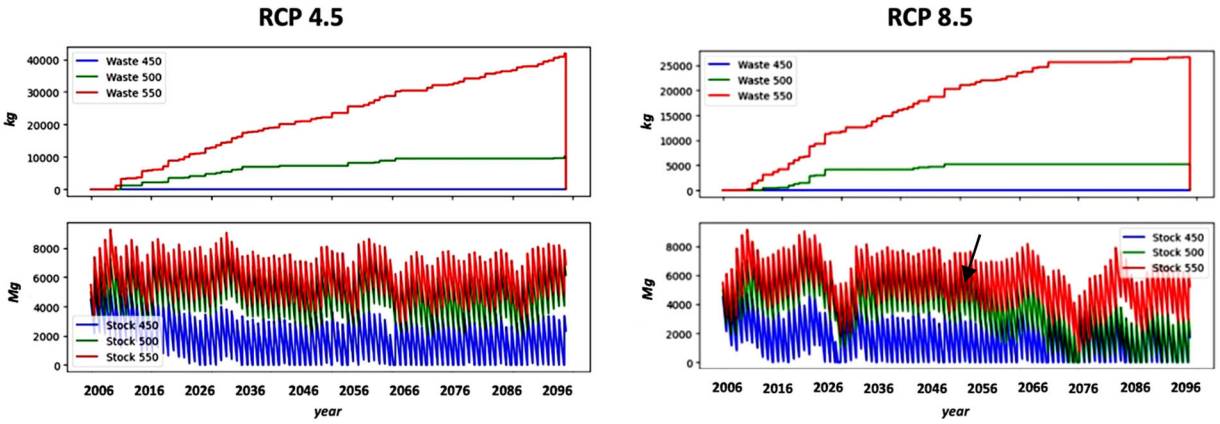

FIGURE 7 Network soybean waste (top plots in kg) and stock accumulation (bottom plots in Mg) during RCP 4.5 and 8.5 climate scenarios with 450, 500, and 550 ha soybean farms. The stock tipping point is denoted with a black arrow. The underlying data for this figure are available in Supporting Information S2.

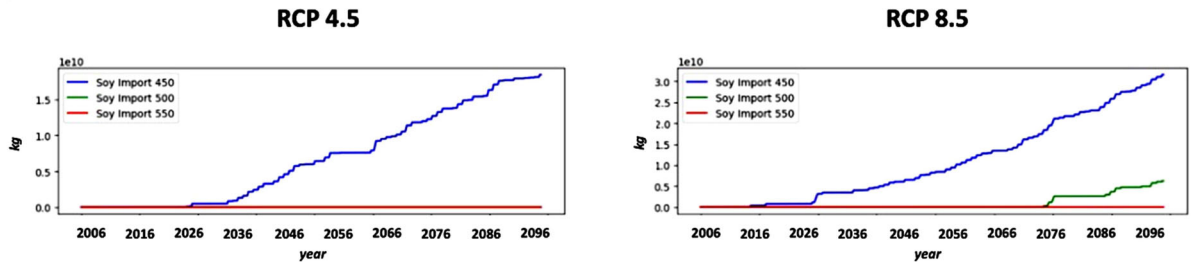

FIGURE 8 Network required import such that production would continue to meet hypothetical demand during RCP 4.5 and 8.5 climate scenarios with 450, 500, and 550 ha soybean farms. The underlying data for this figure are available in Supporting Information S2.

for RCP 8.5, both the 450- and 500-ha farm-supplied networks exhibit failure, with the 500-ha farm-supplied network beginning to fail much later, around 2076.

Similarities do exist between the RCP 4.5 and 8.5 dynamic scenarios shown in Figure 6, with the rate of production failures increasing over time in both. Significant periods with high frequency of failure begin in both scenarios around 2030 and 2060, with denser failure rates shown in the RCP 8.5 scenario.

The cumulative waste generated by each RCP scenario also shows some similarities. In both cases, the 450-ha farm-driven network produces no waste, with the 500 and 550 each producing more, respectively, as shown in Figure 7. However, in both the 500- and 550-ha farm-driven networks, the waste generation in the RCP 4.5 scenario is nearly double that of the RCP 8.5 by the end of the century. Additionally, the waste accumulation plateaus earlier (around 2020) for the 500-ha farm-driven RCP 8.5 scenario than the RCP 4.5 equivalent (around 2030). In the RCP 4.5 scenarios, the 500-ha farm-driven network's waste never begins to plateau but continues linearly throughout the century, whereas in the RCP 8.5 scenario, the waste accumulation follows a logistic slowdown to begin a plateau around 2065. Higher waste accumulation is expected in the RCP 4.5 scenario as crops are less stressed by climate variability and stock accumulation is higher, whereas in the RCP 8.5 scenario, this waste is instead used during periods of lower crop production. This indicates that any capacity expansion during RCP 4.5 to use additional stock may be underutilized if RCP 8.5 scenarios materialize faster, locking in capital investments.

The stock accumulation over time, shown in Figure 7, also reveals some key differences between scenario outcomes. While in both RCP scenarios the 450-ha farm-supplied network stock is the lowest, oscillating around 2000 metric tons (Mg), in the RCP 4.5 scenarios, the 500- and 550-ha farm-supplied stocks follow the same trajectory between 2006 and 2096; in the RCP 8.5 scenarios, a tipping point in stock trajectory occurs around the year 2050. After this point, the 500-ha farm-supplied stock moves to follow the trajectory of the 450-ha farm-supplied stock. The tipping point is followed by a period where the longer-term trajectory of the 550 farm-supplied network stock is also trending toward zero, before rising and following its previous pattern. A similar sharp dipping trend toward zero occurs in the RCP 8.5 scenario for the 500- and 550-ha scenarios around the year 2025, yet no tipping point occurs before or directly after.

The cumulative soybean import required over time required for the network to remain operational (Figure 8) shows further differences between RCP scenarios. While in both scenarios the 550-ha farm-supplied network requires no exogenous import to remain operational throughout the duration of the century, the import required in the 450-ha farm-driven network scenario for RCP 8.5 is nearly double that of RCP 4.5. Furthermore,

while the net import required is linear in the RCP 4.5 scenario, we see a nonlinear increase over time in the RCP 8.5 import. The RCP 8.5 scenario with a 500-ha farm supply also begins to require imports around 2070 (reflecting the failure trend shown in Figure 6).

4 | CONCLUSIONS AND DISCUSSIONS

This work proposes a novel approach to model material flow dynamics in coupled natural–industrial ecosystems using a liquid-time constant machine learning approach for surrogate modeling of material flow dynamics at each node, which are further coupled to evaluate network dynamics.

The results reveal several key insights regarding the resilience and sustainability of the coupled soybean production network in Champaign, Illinois, when subject to different climate change scenarios and farm sizes. Overall, the more extreme RCP 8.5 climate scenario led to an earlier and higher failure frequency across all farm sizes compared to RCP 4.5. This aligns with expectations, as the hotter temperatures and altered precipitation patterns associated with RCP 8.5 are further from the soybean growth optimum. However, the specific timing and frequency of failures varied non-linearly across scenarios and farm sizes, highlighting complex interdependencies. For instance, while the 450-ha farm exhibited no production failures under RCP 4.5, both the 450- and 500-ha farms failed under RCP 8.5. Yet the 500-ha farm did not fail until much later, around 2076. This suggests potential tipping points in the network's dynamics, where smaller farms that were previously resilient begin to fail once climate extremes pass certain thresholds. Larger farms appear to withstand these shifts better initially, but eventually succumb.

The trends in waste accumulation and stock levels reinforce these non-linear behaviors. Under RCP 4.5, waste from the 500- and 550-ha farms increased steadily throughout the century. However, for RCP 8.5, waste for these farms plateaued earlier, around 2020 and 2065, respectively, indicating slowed production. Similarly, the 550-ha farm stock exhibited a precipitous drop around 2050 under RCP 8.5 before recovering, representing a potential tipping point. This alignment between changes in waste, stock, and production failures underscores the value of holistic assessment across the full coupled system.

Notably, the import dependency to sustain production within the network was substantially higher under RCP 8.5 compared to RCP 4.5 for smaller farms. For the 450-ha farm, RCP 8.5 imports were double those for RCP 4.5. This reliance on external inputs to compensate for climate-induced growth constraints reveals vulnerabilities in network resilience. Larger farm-supplied networks were less dependent on imports, but still faced the risk that could manifest in unexpected tipping points.

The LTC algorithmic (inverse model) controllers tuned for the soybean oil and diesel production plants demonstrated proficient tracking of specified production trajectories in response to the dynamic economic demand signal. While not conferring resilience themselves, the controllers enabled continuous operation of the simulated network, linking natural growth variability with industrial processing requirements. Their integration provided a vital mechanism for propagating disruptions across the coupled system to assess impacts on overall production goals. The controller models thus served an important role as open-loop algorithmic constructs facilitating the analysis of resilience and sustainability under different climate scenarios.

One limitation of the soybean growth LTC models for the RCP 4.5 and 8.5 scenarios presented in this work is that these provide insights into potential future growth patterns but do not make definitive predictions. As discussed in the methodology, these models were trained on statistically downscaled climate projections to capture seasonal crop dynamics under hypothetical future warming scenarios. The models exhibited skill in mimicking complex growth patterns and key inflection points. Analysis of model outputs indicates earlier attainment of peak biomass under RCP 8.5 compared to 4.5, suggesting a need to adapt crop timelines. However, the growth models do not account for adaptive measures like shifting sowing dates, alternate crop varieties, or improved agronomic practices. Consequently, their projections should be interpreted as indicative of directional risks, not precise forecasts. Additional integrated modeling is needed to guide specific adaptive management strategies.

Additionally, the current system boundary focuses narrowly on soybean growth, oil production, and biodiesel output in the Champaign, Illinois area. This localized scope enables a tight-coupled physical modeling of the core production chain. However, it likely overlooks important interactions and vulnerabilities that could be included if the scope were to be increased spatially or dimensionally, which is done in other industrial ecology models, such as multi-regional input–output models. Expanding spatially to encompass the broader supply chain for agricultural inputs like seeds, fertilizers, and equipment could reveal single points of failure. If a few key distributors are disrupted, farms across the region could be severely impacted. Transportation networks distributing finished biodiesel are also excluded, masking bottlenecks.

Incorporating crop rotation cycles would uncover potential soil nutrient depletion, pest buildup, and yield declines over successive soybean plantings. Demographic shifts driving urban expansion in the region may also increase pressure on croplands, and competition for water resources with other farms and industries is excluded. This could become critical as climate change alters precipitation and temperature patterns, whose regularity may have historically been taken for granted. Biodiversity impacts on pollinators and natural pest control services are also omitted. Their degradation could dramatically affect yields and require added pesticide inputs. Wider ecosystem impacts of agricultural runoff are similarly overlooked, which can be included by expanding the modeling of ecological systems. Despite these limitations, the proposed approach provides a robust framework to include mechanistic dynamics at nodes to model overall material flow dynamics in a coupled natural–industrial ecosystem, thus advancing the material flow dynamics science in the industrial ecology domain. Future applications include expanding the application for spatial material flow dynamics and identification of climate resilience to the spatially explicit impact of climate change scenarios.

ACKNOWLEDGMENTS

This work was supported in part by the US National Science Foundation through NSF GRFP under grant DGE-1842166 and NSF FMRG Eco 2229250.

CONFLICT OF INTEREST STATEMENT

The authors declare no conflict of interest.

DATA AVAILABILITY STATEMENT

The data that supports the findings of this study are available in the supporting information of this article and submitted in Excel format.

ORCID

Shweta Singh https://orcid.org/0000-0002-0193-9349

REFERENCES

Anjum, M. N., Ding, Y., & Shangguan, D. (2019). Simulation of the projected climate change impacts on the river flow regimes under CMIP5 RCP scenarios in the westerlies dominated belt, northern Pakistan. *Atmospheric Research*, *227*, 233–248. https://doi.org/10.1016/J.ATMOSRES.2019.05.017

Beck, S., & Mahony, M., & W. I. R. Climate, and undefined 2018. (2018). The IPCC and the new map of science and politics. *WIREs Climate Change*, *9*(6), e547. https://doi.org/10.1002/wcc.547

Bekele, W. T., Haile, A. T., & Rientjes, T. (2021). Impact of climate change on the streamflow of the Arjo-Didessa catchment under RCP scenarios. *Journal of Water and Climate Change*, *12*, 2325–2337. https://doi.org/10.2166/wcc.2021.307

Bidollahkhani, M., Atasoy, F., & Abdellatef, H. (2023). LTC-SE: Expanding the potential of liquid time-constant neural networks for scalable AI and embedded systems. http://arxiv.org/abs/2304.08691

Cao, Z., Shen, L., Zhong, S., Liu, L., Kong, H., & Sun, Y. (2018). A probabilistic dynamic material flow analysis model for Chinese urban housing stock. *Journal of Industrial Ecology*, *22*(2), 377–391. https://doi.org/10.1111/JIEC.12579

Cioni, L. (2002). The roles of system dynamics in environmental problem solving. *System Dynamics Review*, *18*(3), 283–296.

Costa, M. H., Yanagi, T., Martins, M. A., & Sentelhas, P. C. (2019). Modeling the potential productivity of soybean under climate change in Brazil. *Science of The Total Environment*, *682*, 155–170.

Davis, C., Nikolić, I., & Dijkema, G. P. J. (2009). Integration of life cycle assessment into agent-based modeling. *Journal of Industrial Ecology*, *13*(2), 306–325. https://doi.org/10.1111/J.1530-9290.2009.00122.X

Dijkema, G. P. J., Xu, M., Derrible, S., & Lifset, R. (2015). Complexity and industrial ecology. *Journal of Industrial Ecology*, *19*(2), 189–194. https://doi.org/10.1111/jiec.12280

Espinoza, V. S., Erbis, S., Pourzahedi, L., Eckelman, M. J., & Isaacs, J. A. (2014). Material flow analysis of carbon nanotube lithium-ion batteries used in portable computers. *ACS Sustainable Chemistry & Engineering*, *2*(7), 1642–1648. https://doi.org/10.1021/SC500111Y

Graedel, T. E. (2019). Material flow analysis from origin to evolution. *Environmental Science & Technology*, *53*(21), 12188–12196. https://doi.org/10.1021/ACS.EST.9B03413

Harirchi, F., Kim, D., Khalil, O., Liu, S., Elvati, P., Baranwal, M., Hero, A., & Violi, A. (2020). On sparse identification of complex dynamical systems: A study on discovering influential reactions in chemical reaction networks. *Fuel*, *279*, 118204.

Hasani, R., Lechner, M., Amini, A., Liebenwein, L., Ray, A., Tschaikowski, M., Teschl, G., & Rus, D. (2022). Closed-form continuous-time neural networks. *Nature Machine Intelligence*, *4*(11), 992–1003. https://doi.org/10.1038/s42256-022-00556-7

Hasani, R., Lechner, M., Amini, A., Rus, D., & Grosu, R. (2020). A natural lottery ticket winner: Reinforcement learning with ordinary neural circuits. *Proceedings of the 37th International Conference on Machine Learning*, *119*, 4082–4093. https://proceedings.mlr.press/v119/hasani20a.html

Hasani, R., Lechner, M., Amini, A., Rus, D., & Grosu, R. (2021). Liquid time-constant networks. *Proceedings of the AAAI Conference on Artificial Intelligence*, *35*(9), 7657–7666. https://doi.org/10.1609/AAAI.V35I9.16936

Huang, Y., Ma, Y., Liu, T., & Luo, M. (2020). Climate change impacts on extreme flows under IPCC RCP Scenarios in the mountainous Kaidu Watershed, Tarim River Basin. *Sustainability*, *12*(5), 2090. https://doi.org/10.3390/SU12052090

José, R. S., Pérez, J. L., González, R. M., Pecci, J., Garzón, A., & Palacios, M. (2016). Impacts of the 4.5 and 8.5 RCP global climate scenarios on urban meteorology and air quality: Application to Madrid, Antwerp, Milan, Helsinki and London. *Journal of Computational and Applied Mathematics*, *293*, 192–207. https://doi.org/10.1016/J.CAM.2015.04.024

Kim, J., Choi, J., Choi, C., & Park, S. (2013). Impacts of changes in climate and land use/land cover under IPCC RCP scenarios on streamflow in the Hoeya River Basin, Korea. *Science of The Total Environment*, *452-453*, 181–195. https://doi.org/10.1016/J.SCITOTENV.2013.02.005

Lechner, M., Hasani, R., Amini, A., Henzinger, T. A., Rus, D., & Grosu, R. (2020). Neural circuit policies enabling auditable autonomy. *Nature Machine Intelligence*, *2*, 642–652. https://doi.org/10.1038/s42256-020-00237-3

Meerow, S., Newell, J. P., & of I. Ecology, and undefined 2015. (2015). Resilience and complexity: A bibliometric review and prospects for industrial ecology. *Wiley Online Library*, *19*(2), 236–251. https://doi.org/10.1111/jiec.12252

Meinrenken, C. J., Sauerhaft, B. C., Garvan, A. N., & Lackner, K. S. (2014). Combining life cycle assessment with data science to inform portfolio-level value-chain engineering. *Journal of Industrial Ecology*, *18*(5), 641–651. https://doi.org/10.1111/JIEC.12182

Müller, D. B., Bader, H. P., & Baccini, P. (2004). Long-term coordination of timber production and consumption using a dynamic material and energy flow analysis. *Journal of Industrial Ecology*, *8*(3), 65–88. https://doi.org/10.1162/1088198042442342

Nabavi, E., Daniell, K. A., & Najafi, H. (2018). Boundary matters: The potential of system dynamics to support sustainability? *Sustainability Science*, *13*(1), 47–63.

Nasonova, O. N., Gusev, Y. M., Kovalev, E. E., & Ayzel, G. V. (2018). Climate change impact on streamflow in Large-Scale River Basins: Projections and their uncertainties sourced from GCMs and RCP scenarios. *Proceedings of the International Association of Hydrological Sciences*, *379*, 139–144. https://doi.org/10.5194/PIAHS-379-139-2018

Nilawar, A. P., & Waikar, M. L. (2019). Impacts of climate change on streamflow and sediment concentration under RCP 4.5 and 8.5: A case study in Purna river basin, India. *Science of The Total Environment*, *650*, 2685–2696. https://doi.org/10.1016/J.SCITOTENV.2018.09.334

Padhiary, M., Hoque, A., Prasad, G., Kumar, K., & Sahu, B. (2025). Precision agriculture and AI-driven resource optimization for sustainable land and resource management. In *Smart water technology for sustainable management in modern cities* (pp. 197–231). https://doi.org/10.4018/979-8-3693-8074-1.CH009

Padhiary, M., & Kumar, R. (2024). Assessing the environmental impacts of agriculture, industrial operations, and mining on agro-ecosystems. *Studies in Computational Intelligence*, *1165*, 107–126. https://doi.org/10.1007/978-3-031-70102-3_8

Pauliuk, S., Majeau-Bettez, G., & Müller, D. B. (2015). A general system structure and accounting framework for socioeconomic metabolism. *Journal of Industrial Ecology*, *19*(5), 728–741. https://doi.org/10.1111/JIEC.12306

Riahi, K., Rao, S., Krey, V., Cho, C., Chirkov, V., Fischer, G., Kindermann, G., Nakicenovic, N., & Rafaj, P. (2011). RCP 8.5—A scenario of comparatively high greenhouse gas emissions. *Climatic Change*, *109*(1–2), 33–57.

Rivera, D. E. (1996). System identification in the process industries. *Automatica*, *32*(12), 1661–1676.

Rivera, D. E., Lee, H., Braun, M. W., & Mittelmann, H. D. (2003). "Plant-Friendly" system identification: A challenge for the process industries. *IFAC Proceedings Volumes*, *36*(16), 891–896.

Rogelj, J., Meinshausen, M., & Knutti, R. (2012). Global warming under old and new scenarios using IPCC climate sensitivity range estimates. *Nature Climate Change*, *2*(4), 248–253. https://doi.org/10.1038/nclimate1385

Sendra, C., Gabarrell, X., & Vicent, T. (2007). Material flow analysis adapted to an industrial area. *Journal of Cleaner Production*, *15*(17), 1706–1715. https://doi.org/10.1016/J.JCLEPRO.2006.08.019

Streeck, J., Pauliuk, S., Wieland, H., & Wiedenhofer, D. (2023). A review of methods to trace material flows into final products in dynamic material flow analysis: From industry shipments in physical units to monetary input–output tables, Part 1. *Journal of Industrial Ecology*, *27*(2), 436–456. https://doi.org/10.1111/JIEC.13380

Wang, J., Hu, L., Li, D., & Ren, M. (2020). Potential impacts of projected climate change under CMIP5 RCP scenarios on streamflow in the Wabash River Basin. *Advances in Meteorology*, *2020*, 1–18.

Xu, Y., Geng, Y., Tian, X., Shen, W., & Gao, Z. (2024). Uncovering the key features of platinum metabolism in China during 2001–2022: A dynamic material flow analysis. *Journal of Cleaner Production*, *446*, 141323. https://doi.org/10.1016/j.jclepro.2024.141323

Zhang, Y., You, Q., Chen, C., & Ge, J. (2016). Impacts of climate change on streamflows under RCP scenarios: A case study in Xin River Basin, China. *Atmospheric Research*, *178-179*, 521–534. https://doi.org/10.1016/J.ATMOSRES.2016.04.018

SUPPORTING INFORMATION

Additional supporting information can be found online in the Supporting Information section at the end of this article.

How to cite this article: Farlessyost, W., & Singh, S. (2025). Modeling material flow dynamics in coupled natural-industrial ecosystems for resilience to climate change: A case study on a soybean-based industrial ecosystem. *Journal of Industrial Ecology*, *29*, 1882–1896. https://doi.org/10.1111/jiec.70087